

## Ca-modified Al–Mg–Sc alloy with high strength at elevated temperatures due to a hierarchical microstructure

Du, Haiquan; Zhang, Shasha; Zhang, Bingyi; Tao, Xuewei; Yao, Zhengjun; Belov, Nikolay; van der Zwaag, Sybrand; Liu, Zili

**DOI**

[10.1007/s10853-021-06310-5](https://doi.org/10.1007/s10853-021-06310-5)

**Publication date**

2021

**Document Version**

Final published version

**Published in**

Journal of Materials Science

**Citation (APA)**

Du, H., Zhang, S., Zhang, B., Tao, X., Yao, Z., Belov, N., van der Zwaag, S., & Liu, Z. (2021). Ca-modified Al–Mg–Sc alloy with high strength at elevated temperatures due to a hierarchical microstructure. *Journal of Materials Science*, 56(28), 16145-16157. <https://doi.org/10.1007/s10853-021-06310-5>

**Important note**

To cite this publication, please use the final published version (if applicable).  
Please check the document version above.

**Copyright**

Other than for strictly personal use, it is not permitted to download, forward or distribute the text or part of it, without the consent of the author(s) and/or copyright holder(s), unless the work is under an open content license such as Creative Commons.

**Takedown policy**

Please contact us and provide details if you believe this document breaches copyrights.  
We will remove access to the work immediately and investigate your claim.

***Green Open Access added to TU Delft Institutional Repository***

***'You share, we take care!' - Taverne project***

**<https://www.openaccess.nl/en/you-share-we-take-care>**

Otherwise as indicated in the copyright section: the publisher is the copyright holder of this work and the author uses the Dutch legislation to make this work public.



# Ca-modified Al–Mg–Sc alloy with high strength at elevated temperatures due to a hierarchical microstructure

Haiquan Du<sup>1,2</sup>, Shasha Zhang<sup>1,2,\*</sup> , Bingyi Zhang<sup>1,2</sup>, Xuewei Tao<sup>3</sup>, Zhengjun Yao<sup>1,2</sup>, Nikolay Belov<sup>4</sup>, Sybrand van der Zwaag<sup>5</sup>, and Zili Liu<sup>1</sup>

<sup>1</sup> College of Materials Science and Technology, Nanjing University of Aeronautics and Astronautics, Nanjing 210016, China

<sup>2</sup> Key Laboratory of Materials Preparation and Protection for Harsh Environment, Ministry of Industry and Information Technology, Nanjing 210016, China

<sup>3</sup> School of Materials Science and Engineering, Nanjing Institute of Technology, Nanjing 211167, China

<sup>4</sup> National University of Science and Technology MISIS, 4 Leninsky pr, Moscow, Russia 119049

<sup>5</sup> Novel Aerospace Materials group, Faculty of Aerospace Engineering, Delft University of Technology, Delft, the Netherlands

Received: 23 April 2021

Accepted: 1 July 2021

Published online:

9 July 2021

© The Author(s), under exclusive licence to Springer Science+Business Media, LLC, part of Springer Nature 2021

## ABSTRACT

Al–Mg alloys are normally prone to lose part of their yield and tensile strength at high temperatures due to insufficient thermal stability of the microstructure. Here, we present a Ca-modified Al–Mg–Sc alloy demonstrating high strength at elevated temperatures. The microstructure contains Al<sub>4</sub>Ca phases distributed as a network along the grain boundary and Al<sub>3</sub>(Sc,Zr) nano-particles dispersed within the grains. The microstructure evolution and age-hardening analysis indicate that the combination of an Al<sub>4</sub>Ca network and Sc-rich nano-particles leads to excellent thermal stability even upon aging at 300 °C. The tensile strength of the alloy for temperatures up to 250 °C is significantly improved by an aging treatment and is comparable with the commercial heat-resistant aluminum alloys, i.e., A356 and A319. At a high temperature of 300 °C, the tensile strength is superior to the above-mentioned commercial alloys, even more so when expressed as the specific strength due to the low density of Ca-modified Al–Mg–Sc alloy. The excellent high-temperature strength results from a synergistic effect of solid solution strengthening, grain boundary strengthening and nanoparticle order strengthening.

Handling Editor: P. Nash.

Address correspondence to E-mail: s.zhang@nuaa.edu.cn

<https://doi.org/10.1007/s10853-021-06310-5>

## Introduction

With the sustained development of automotive and aerospace industries, more stringent requirements for high-temperature resistance and high specific strength have been formulated to meet the application targets [1–3]. For example, heat-resistant cast aluminum alloys are widely used in automobile engine blocks and pistons to replace cast iron, due to their low density and outstanding (specific) mechanical properties [4, 5]. In recent years, heat-resistant aluminum alloys have become a research topic hotspot in various countries. Researchers have significantly improved the high-temperature performance of aluminum alloys by adding alloying elements to improve alloy properties as well as its processability [5–10]. For example, in the research of heat-resistant Al–Si and Al–Cu cast alloys, traces of rare earth elements (such as Ce, Gd, Er, etc.) or transition metal elements (such as Ag, Co, Cr, Y, etc.) have been added to form high-temperature stable nano precipitates. Such precipitates pin grain boundaries and dislocations and, as they barely coarsen, improve the heat resistance [11–16].

Aluminum alloys with magnesium (Mg) as its major alloying element are widely used in automotive, maritime, aerospace and other fields due to their medium strength, high ductility, excellent corrosion resistance, weldability and excellent processing performance [17, 18]. However, since the eutectic temperature of the Al–Mg system is low (450 °C), these alloys are prone to soften significantly at high temperature and their heat resistance is classified as relatively poor [18]. Hence, the traditional Al–Mg alloys cannot be used as structural materials at high temperatures. However, Vo et al. found that the formation of nano-precipitates with the  $L1_2$  structure, i.e.,  $Al_3Sc$ ,  $Al_3(Sc,Zr)$ ,  $Al_3(Er,Zr)$ , can significantly enhance the heat resistance [19]. The precipitates play a role in refining the microstructure, inhibiting recrystallization and were demonstrated to be stable as coherent or semi-coherent precipitates in the matrix [17, 20–22]. However, only small amounts of rare earth elements like Sc, Er will be added as the material costs are high and they may lead to the formation of undesirable coarse primary phases at higher concentrations. Hence, the realizable high-temperature strengthening effect due to such nano-precipitates is limited [23, 24].

In recent years, researchers have also found that intermetallic compounds can meaningfully affect the high-temperature strength of aluminum alloys. Intermetallic compounds with a high thermal stability and forming a three-dimensional network structure in the matrix played a key role in improving the strength at high temperatures [16, 25]. One of the elements to be considered is Ca as it has a low density, is abundantly available and the eutectic temperature of (Al) +  $Al_4Ca$  is relatively high at 617 °C (7.6wt%) [26, 27]. However, there are few studies on the application of Ca in aluminum alloys [28–30]. In recent years, Belov et al. developed Al–Ca–Sc, Al–Ca–Mn–Fe and Al–Zn–Mg–Ca alloys, which promoted the development and application of Al–Ca alloys [31–34]. However, the combination of (high temperature) strengthening due to rare earth precipitates and Ca-based intermetallics has not been explored yet.

Hence, in this study, the microstructure and high-temperature mechanical properties of Al–Mg–Sc–Zr–Mn alloy modified with Ca will be investigated. The purpose of this studies is to provide a new alloy concept for the enhancement of the heat resistance of cast aluminum alloys based on hierarchical multi-phase synergetic effects.

## Experimental procedures

### Materials

The alloy was prepared starting with high-purity aluminum (Al) (99.99%). Ca and magnesium (Mg) were added in pure metallic form, scandium (Sc), zirconium (Zr) and manganese (Mn) were added as Al-2% Sc, Al-10% Zr and Al-10% Mn master alloys. The smelting was carried out in a vacuum melting furnace. After being held between 730 and 760 °C for 30 min, the alloy was cast into a preheated cylindrical copper mold (120 mm in diameter and 250 mm in height). The chemical composition of the alloy as determined by ICP-OES (Agilent 720ES) is given in Table 1. The samples were cut from the center of ingot, and heat treatments were carried out in an electric muffle furnace. The age-hardening investigation was carried out at temperatures ranging from 300 to 450 °C. The high-temperature stability of the microstructure was studied using double aging

**Table 1** Chemical composition (wt.%) of the experimental alloy

Element	Al	Mg	Ca	Sc	Zr	Mn	Others
Concentration	Balance	4.82	0.89	0.51	0.21	0.54	< 0.04

annealing treatment, first aging at 300 °C for 4 h, followed by annealing at 500 °C for 36 h.

## Characterization of microstructures and mechanical properties

Heat-treated samples were ground and mechanically polished, followed by electrochemical polishing (perchloric acid: alcohol 1:9) and etching with Keller's reagent (hydrochloric acid 1.5%, hydrofluoric acid 1%, nitric acid 2.5% and distilled water 95%). The microstructures were studied using optical microscopy (OM, Olympus inverted metallurgical microscope GX51) and scanning electron microscopy (SEM, JSM-7600F, JEOL, Japan). Grain sizes were determined using the linear intercept method, according to the GB/T 6394-2017 test protocol. Energy-dispersive X-ray spectroscopy (EDS) was used to determine the spatial distribution of chemical elements in the specimens and the composition of the phases. Samples were also characterized using X-ray diffraction (XRD) with a Cu K $\alpha$  radiation at 40 mA and 40 kV (Smartlab 9KW). Diffraction angles ( $2\theta$ ) ranged from 20° to 80°. Measurements were made at a scan speed of 2° per minute. Transmission electron microscopy (TEM, JEM 2100) was employed for determining the crystal structure of the nano-phase existing in the alloy. The Vickers hardness of the samples was measured using a Vickers microhardness tester (FM-700) at a load of 100 g and an indentation time of 20 s. Tensile tests were carried out at room temperature on a CMT5205 testing machine (MTS industrial systems, China) at a fixed strain rate of 1 mm/min. Mechanical properties at elevated temperatures were measured on a CMT5808 testing machine (MTS industrial systems, China) using the GB/T 228.2 test protocol. Fracture surfaces of samples tested at room and elevated temperatures were further studied using SEM.

## Phase diagram calculation

The phase composition of the Al–Mg–Sc–Zr–Mn–Ca system was calculated using the Thermo-Calc program in combination with the TTAL5 database to facilitate the preliminary analysis.

## Results

### Microstructure characterization

The equilibrium phase composition of the Ca-modified Al–Mg–Sc alloy can be seen in the polythermal section calculated at 5 wt % Mg, 0.5 wt % Sc, 0.2 wt % Zr, 0.5 wt % Mn and Ca (0~6 wt %). As follows from Fig. 1, the appearance of primary crystals of the Al<sub>3</sub>(Sc,Zr) phase should be expected. And it can be seen that, under the equilibrium conditions, for the designed alloy composition (Ca about 1wt %) the alloy system only contains the phases of binary systems, i.e., Al<sub>4</sub>Ca, Al<sub>3</sub>(Sc,Zr) and Al<sub>6</sub>Mn at temperatures above 300 °C.

Optical and scanning electron microscopy images of the samples in various heat-treated stages are shown in Figs. 2 and 3, respectively. The Al<sub>4</sub>Ca phase forming a network (or semi-network) structure can be observed at the grain boundaries. In addition, primary Al<sub>3</sub>(Sc,Zr) crystals with a polyhedral shape,

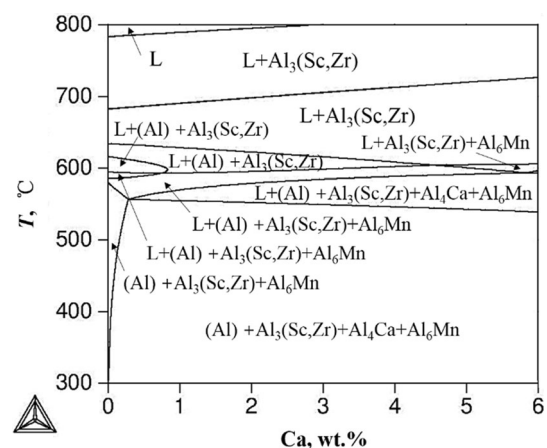


**Figure 1** Vertical section of Al–Mg–Sc–Zr–Mn–Ca system at 5%Mg, 0.5%Sc, 0.2%Zr and 0.5%Mn (wt.%).

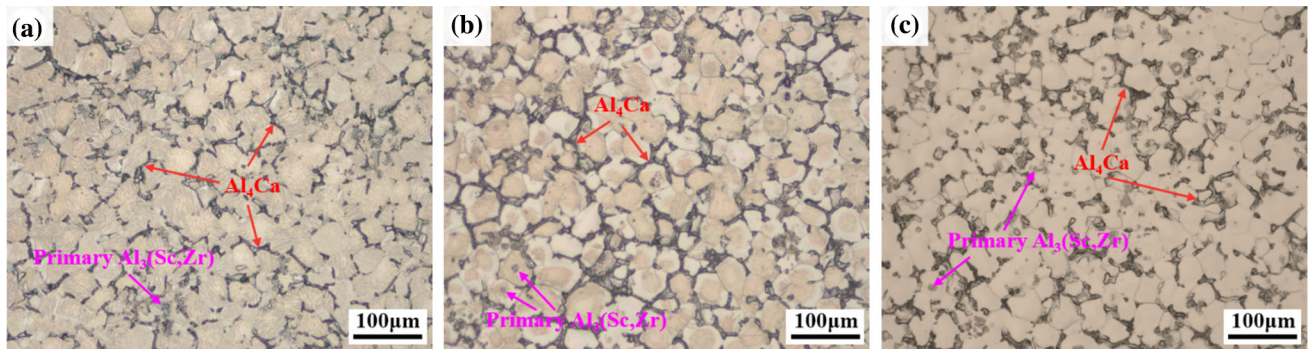


**Figure 2** Optical micrograph of specimens, **a** as-cast state, **b** aged at 300 °C for 4h, **c** aged at 300 °C for 36h.

characteristic for binary Al–Sc alloys [35, 36], were observed.

The  $\text{Al}_3(\text{Sc,Zr})$  particles have a higher solidification temperature and acted as nucleants [37], reducing the growth of  $\alpha$ -Al dendrites and playing a role in refining the grain structure. The  $\text{Al}_4\text{Ca}$  phase is formed at the later stage of the solidification process. As the mass fraction of Ca in the liquid increases,  $\text{Al}_4\text{Ca}$  solidifies at the grain boundaries, thus forming a network structure. Previous research has shown that the volume fraction of the network  $\text{Al}_4\text{Ca}$  increases with increasing Ca content, but at high Ca concentrations the network structure coarsens and even cracks, which is fatal for the mechanical properties [30]. For the current sample with a low Ca concentration, no coarse features in the network nor microcracks were found.

Figures 2 and 3 also show the microstructures of Al–Mg–Sc–Ca alloy after aging at the two aging conditions (aged at 300 °C for 4h and aged at 300 °C for 36h). It can be observed that with increasing aging time, the network structure of the  $\text{Al}_4\text{Ca}$  phase remained like that of the as-cast samples and did not change significantly. Even after aging at 450 °C for 36 hours, no changes in the morphology of  $\text{Al}_4\text{Ca}$ , indicative of granular transformation or spheroidization [32, 38], were observed. Only a small amount of short rod-shaped newly formed precipitates was recorded, as shown in Fig. 3g, h, and these were classified as  $\text{Al}_6\text{Mn}$  [39]. The good thermal stability of  $\text{Al}_4\text{Ca}$  is mainly due to its high eutectic temperature (617 °C). On the other hand, the fineness of the as-cast eutectic structure also determines the likelihood of a morphology change during a heat treatment. In this alloy, the lateral dimensions of the  $\text{Al}_4\text{Ca}$  are a little bigger than those reported in other

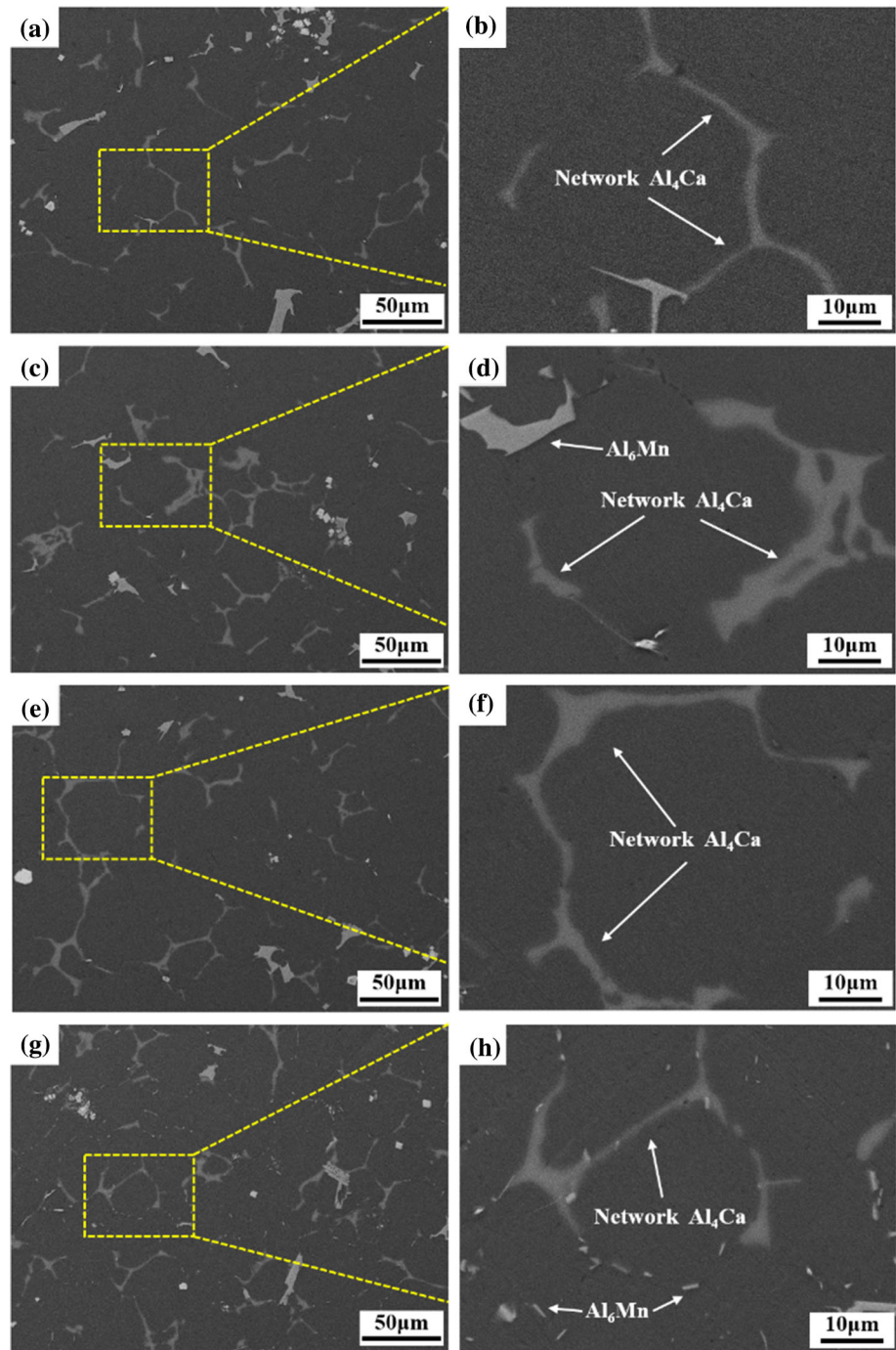
Al–Ca alloys [32, 38]. The thickness of the  $\text{Al}_4\text{Ca}$  crystals is about 1–2  $\mu\text{m}$ .

We also studied the dependence of grain size on conditions of the aging treatment. The grain size of the cast alloy is about  $32.0 \pm 1.5 \mu\text{m}$ . After aging at 300 °C  $\times$  4h + 500 °C  $\times$  36h, the grain size was found to be  $33.9 \pm 2.3 \mu\text{m}$  indicative of an excellent thermal stability and the absence of grain growth. It is attributed to the pinning effect of  $\text{Al}_3(\text{Sc,Zr})$  particles in combination with the high thermal resistance of the  $\text{Al}_4\text{Ca}$  network itself.

According to the EDS results shown in Fig. 4, Ca is mainly present near the grain boundaries, and the Ca distribution does not change during the aging treatment. Thermodynamic calculations have indicated that Ca should not form ternary eutectic phases with the other alloying elements Mg, Sc and Zr [32]. The detailed compositions of areas marked by the named crosses in Fig. 4a, c are listed in Table 2. The network structure is mainly composed of Al and Ca, and its atomic ratio is close to 4:1, which can be identified as  $\text{Al}_4\text{Ca}$  phase. Moreover, no Sc and Zr were found in  $\text{Al}_4\text{Ca}$  eutectic tissue, which is consistent with published research. In addition to the  $\text{Al}_4\text{Ca}$  distributed in the network structure, a small amount of  $\text{Al}_6\text{Mn}$  was precipitated at the grain boundaries [39].

The XRD spectra of the Ca-modified Al–Mg–Sc specimens in their cast and aged states are shown in Fig. 5. The diffraction peaks corresponding to face-centered cubic (fcc)  $\alpha$ -Al (JCPDS Card No. 04–0787) were detected for all specimens. The  $\text{Al}_4\text{Ca}$  phase was easily identified, and the primary phases  $\text{Al}_3\text{Sc}$  and  $\text{Al}_6\text{Mn}$  were also detected in the XRD diffractograms, which is consistent with the results from SEM (Figs 3 and 4). Upon aging, there is no change in the phase characteristics. Figure 5b shows the comparison of the standard  $\alpha$ -Al diffraction peak at  $2\theta =$

**Figure 3** SEM images of samples at different states, **a** as-cast state, **c** aged at 300 °C for 4h, **e** aged at 300 °C for 36h, **g** aged at 450 °C for 36h; **b**, **d**, **f** and **h** are high magnification of fig **a**, **c**, **e**, **g**, respectively.



38.37° with the measured results. The shift in the characteristic peaks of the  $\alpha$ -Al matrix is attributed to Mg being in solid solution. No obvious signs of a strong texture were observed or expected.

The structure of the alloy after aging at 300°C for 4h was studied in more detail by TEM, and Figure 6 shows the typical structure of  $\text{Al}_3(\text{Sc,Zr})$  nano-particles precipitated during aging, which is consistent

with published studies on Al–Sc–Zr alloys [40]. Upon aging, the Sc-rich particles (Fig. 6b) remain spheroidal, coherent and uniformly distributed in the matrix. And Fig. 6c also shows the  $\text{Al}_6\text{Mn}$  phase.

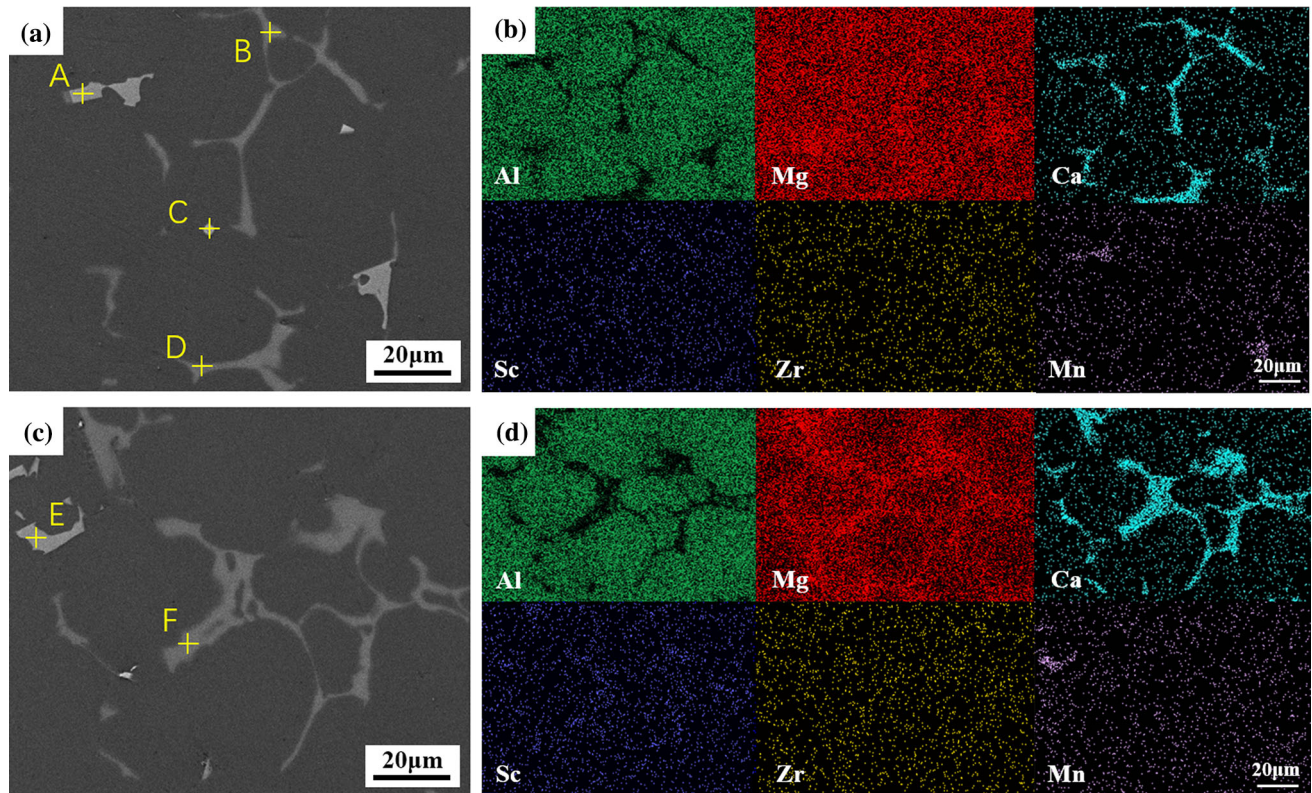


**Figure 4** EDS mapping of samples, **a** microstructure of as-cast state, **b** EDS mapping showing Al, Mg, Ca, Sc, Zr and Mn of **a**, **c** microstructure of aged at 300°C for 4h, **d** EDS mapping of (c).

**Table 2** Local chemical composition as determined by EDS point analysis at the locations marked in Fig 4a and Fig 4c

Element	Mg(at.%)	Ca(at.%)	Sc(at.%)	Zr(at.%)	Mn(at.%)	Al(at.%)
A	0.61	11.09	–	–	18.00	70.30
B	0.76	17.57	–	–	–	81.67
C	1.32	0.80	13.72	6.89	–	77.27
D	1.73	29.68	–	–	–	68.59
E	0.74	9.72	–	–	24.00	65.54
F	0.53	22.64	–	–	0.29	76.54

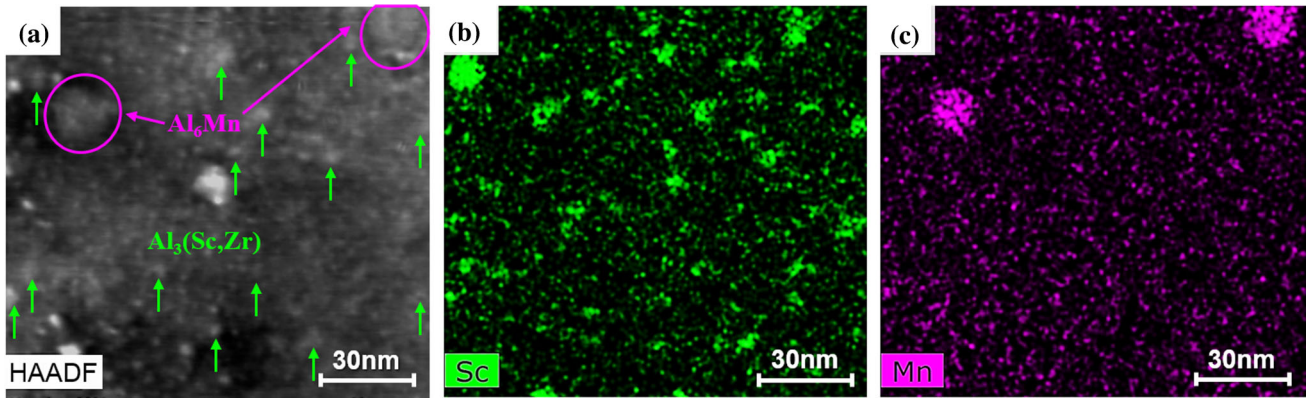
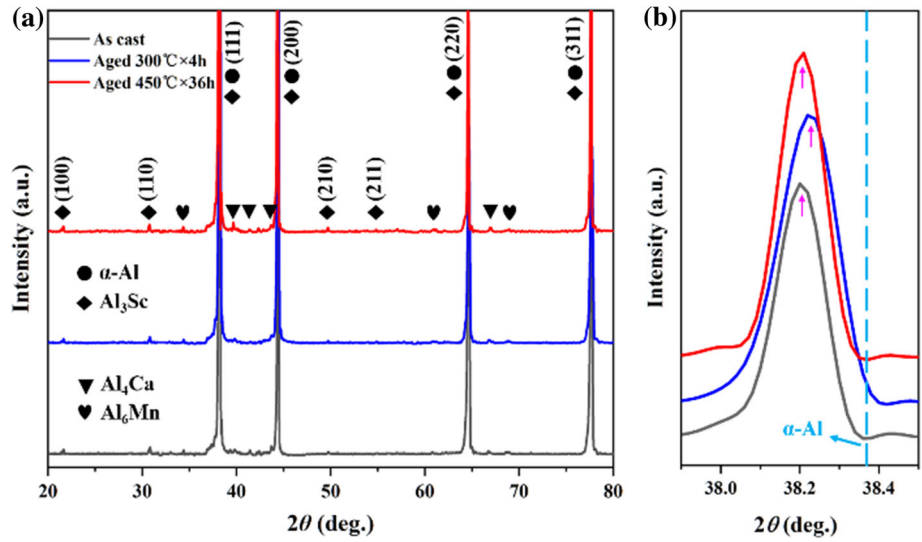
## Mechanical properties

The evolution of the Vickers microhardness as a function of the aging time over the temperature range of 300 ~ 450 °C is shown in Fig. 7. The microhardness test locations were chosen in the middle of the grains to prevent grain boundaries effects to interfere with the test results. It can be seen that a maximum microhardness of 118 HV is achieved upon aging at 300 °C for 16h, and this value is more than 20% higher than that in the cast state (97 HV). The increase is due to the precipitation of  $Al_3(Sc,Zr)$  nano-particles. As the TEM images shown in Fig. 6 reveal the  $Al_3(Sc,Zr)$  nano-particles are nicely dispersed and

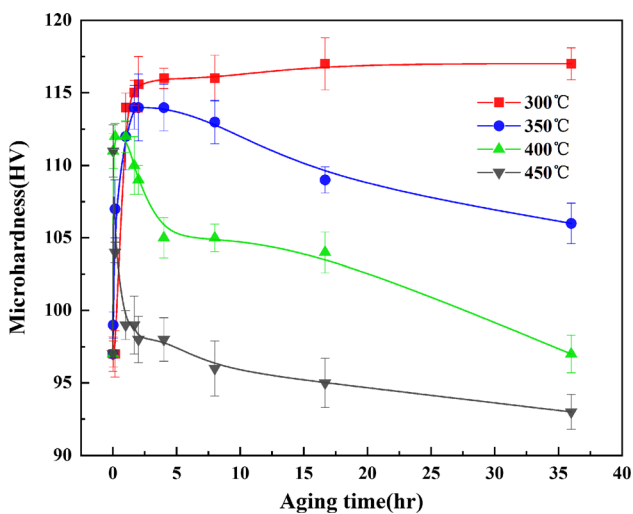
have a size of about 4–9 nm. The peak hardness of the alloy decreases with increasing aging temperature. With increasing aging temperature, the time for the hardness to reach the peak value is shortened, and as a result of particle coarsening the hardness decreases more rapidly after reaching the peak hardness. According to the literature, significant  $Al_3(Sc,Zr)$  nano-particles coarsening only occurs above 450°C accompanied by a sharp decrease in particle density, leading to a much weakened strengthening effect [41]. After aging at 450 °C for 36 h, the hardness is even lower than that of the samples in the cast state.

Figure 8a shows representative stress-strain curves of the samples in aged and as-cast state (insert) tested

**Figure 5** **a** XRD results of Ca-modified Al–Mg–Sc specimens at different states, **b** XRD spectra in the vicinity of the standard diffraction peak of  $\alpha$ -Al phase ( $2\theta = 38.37^\circ$ ).



**Figure 6** TEM images of the microstructure of the alloy aged at 300°C for 4h, **a** STEM HAADF images of  $Al_3(Sc,Zr)$  nano-particles and  $Al_6Mn$ , **b**, **c** corresponding Sc and Mn EDX mapping from (a), respectively.



**Figure 7** Microhardness-time curves for the Ca-modified Al–Mg–Sc alloy aged at 300 °C ~ 450 °C.

at 150 °C, 250 °C and 300 °C. Per conditions, at least three samples were tested. The dependences of the ultimate tensile strength (UTS), the yield strength (YS) and the specific strength on testing temperatures are given in Figs. 8b–f (marked with dotted lines), respectively, with detailed values provided in Table 3. Upon aging, the UTS at room temperature increased from 211 to 253MPa. It can be concluded that the YS and UTS of the specimens after aging heat treatment are significantly higher than those of the cast samples tensile tested at the same temperature. The UTS at 150 °C of the aged alloy is higher than that at room temperature, reaching a value of 259 MPa. But the tensile strength decreases with the further increase of temperature, yet remains at a high value of 136 MPa and 133MPa at 300 °C for the cast and heat-treated condition, respectively. The elongation of the samples increased with increasing test

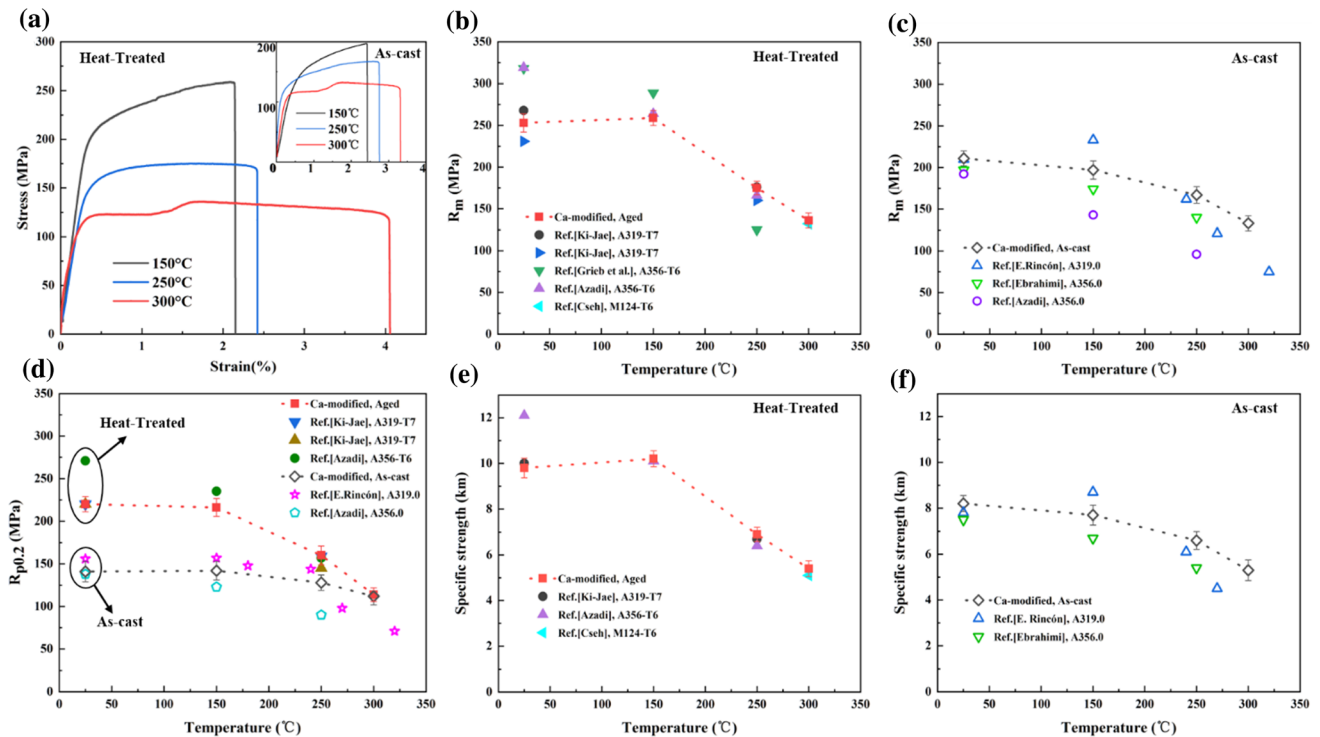


**Figure 8** a Characteristic tensile stress-strain curves of the Ca-modified Al–Mg–Sc alloy in aged and cast state (insert) at three temperatures, b, c the ultimate tensile stress of heat-treated and as-

cast alloys versus the temperature, respectively, d yield stress values versus the temperature, e, f the specific strength of heat-treated and as-cast alloys versus the temperature, respectively.

**Table 3** True ultimate tensile strength  $R_m$ , yield strength  $R_{p0.2}$  and fracture elongation  $\delta$  of specimens

Alloys	Temp (°C)	$R_m$ (MPa)	$R_{p0.2}$ (MPa)	$\delta$ (%)
As-cast	25	211	141	2.5
	150	197	142	2.4
	250	167	128	2.7
	300	133	112	3.3
	350	73	72	10.4
Aged at 300°C for 4h	25	253	220	2.0
	150	259	216	2.2
	250	175	160	2.4
	300	136	114	4.1
	350	70	69	17.1

temperature, and rose from 2 to 5% at room temperature to 17.1% at 350 °C.

The UTS, YS and specific strength of the current alloy are also compared with the values for conventional and commercial heat-resisting aluminum alloys, i.e., A356, A319 and M124, as shown in Fig. 8d–f, respectively [42–47]. Compared with A356 and A319 alloys, the UTS of Ca-modified alloy in aging states is lower at room temperature and 150 °C, but better at 250 °C and higher temperatures, and even higher than that of M124 at 300 °C. And the UTS

of Ca-modified alloy in cast states are higher than the others, except at 150 °C, lower than that of A319. Similarly, the YS and specific strength are higher at elevated temperatures than that of the commercial grades. In addition, all mechanical properties of A356 alloy are reduced significantly with increasing test temperature [44]. The UTS and YS of cast samples dropped by 25% and 11% when going from room temperature to 150 °C, respectively, and dropped by 17% and 13%, respectively, for the aged samples. Especially, when the test temperature is higher than

250 °C, this reduction is more significant. However, we unexpectedly observed that the UTS and YS values of our Ca-modified new alloy did not decrease at 150 °C with respect to the room temperature values. And at higher temperatures, the decrease in tensile strength for both the cast and aged state is modest compared to that in A356 and A319 alloys. Due to the low atomic mass of Ca, the samples with Ca addition have a higher specific strength at elevated temperatures. In addition, the temperature-dependent fracture elongation of the new alloy (Table 3) is always equal or better than that published for the A319 alloy [45].

During the tensile tests at room temperature and at elevated temperatures, no obvious signs of necking were observed. To further clarify the fracture mechanism, Fig. 9 shows the fracture morphology of specimens. The fracture surface of all the specimens was relatively rough. The fracture of the alloy broken at room temperature is characterized by quasi-cleavage fracture of a brittle nature. With increasing temperature, more dimples appeared, but there were still many cleavage planes and tearing edges, indicative of a transition from brittle fracture to ductile fracture. At the highest test temperature, the fracture mode of the alloy is quasi-cleavage fracture dominated by ductile fracture. This is consistent with the elongation data from the tensile tests.

### Discussion

The superior strength properties for the Ca-modified Al–Mg–Sc alloys are the result of the additive effects of multiple strengthening mechanisms.

It has been shown that the yield strength depends on the cumulative effects of solid solution

strengthening ( $\sigma_{ss}$ ), grain boundary strengthening ( $\sigma_{GB}$ ) and particle strengthening ( $\sigma_{ppt}$ ). Therefore, the yield strength can be expressed by:

$$\sigma_y = \sigma_{ss} + \sigma_{GB} + \sigma_{ppt} \tag{1}$$

The solid solution strengthening is given by [17]:

$$\sigma_{ss} = \frac{3.1\varepsilon Gc^{1/2}}{700} \tag{2}$$

where  $\varepsilon$  is an experimental constant, and is estimated to be 0.38 for Mg in Al–Mg alloy [18],  $G$  is the shear modulus of the  $\alpha$ -Al, 25.4 GPa at room temperature [48], and  $c$  is the concentration of solute in at.%. Considering the amount of Mg in solid solution, the strength increment is calculated to be 74 ~ 85 MPa.

The dependence of the yield strength on the average grain boundary diameter ( $d$ ) can be expressed by Hall-Petch relationship [18]:

$$\sigma_{GB} = \sigma_0 + kd^{-1/2} \tag{3}$$

where  $\sigma_0$  is the intrinsic resistance of the lattice to dislocation motion, and is approximately 20 MPa for most aluminum alloys, and  $k$  is the constant representing the relative strengthening contribution from grain boundaries, and is usually taken to be 0.14 MN/m<sup>3/2</sup> [49]. The estimated strength increment due to the grain size effect is 44 ~ 45 MPa.

Strengthening of the alloy due the presence of Al<sub>3</sub>(Sc,Zr) particles was analyzed by considering order strengthening, coherency strengthening, and Orowan particle strengthening models [19, 41, 50]. The order strengthening,  $\sigma_{ord}$ , is given by:

$$\sigma_{ord} = 0.81M \frac{\gamma_{APB}}{2b} \left(\frac{3\pi\theta}{8}\right)^{1/2} \tag{4}$$

where  $M = 3.06$  is the mean matrix orientation factor for Al,  $b = 0.286$  nm is the magnitude of the matrix

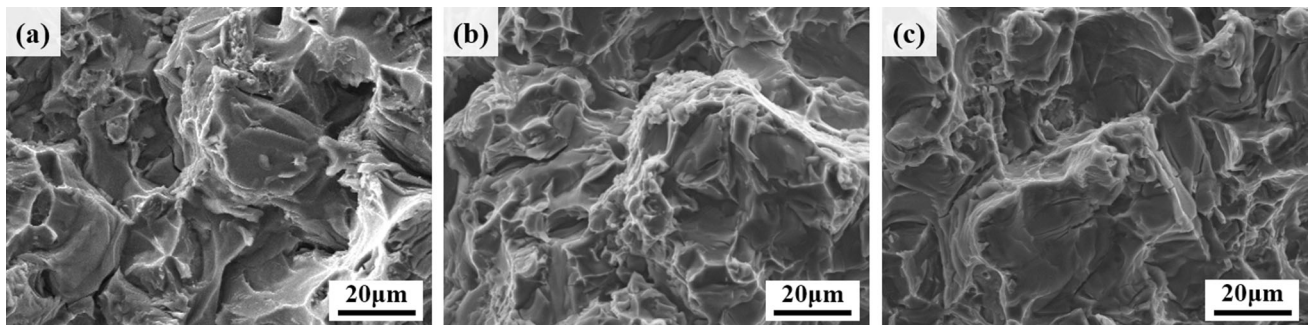


**Figure 9** Fracture surfaces of Ca-modified Al–Mg–Sc specimens aged at 300 °C for 4h, **a** tested at room temperature, **b** at 150 °C, **c** at 300 °C.

Burgers vector,  $\theta$  is the volume fraction of precipitates measured by TEM, and  $\gamma_{\text{APB}} = 0.5 \text{ J m}^{-2}$  is an average value of the  $\text{Al}_3\text{Sc}$  anti-phase boundary energy for the (111) plane [49]. Coherency strengthening,  $\sigma_{\text{coh}}$ , is calculated as:

$$\sigma_{\text{coh}} = M\alpha_{\varepsilon}(G\theta)^{3/2}\left(\frac{r\theta}{0.5Gb}\right)^{1/2} \quad (5)$$

where  $\alpha_{\varepsilon} = 2.6$  is a constant,  $r$  is the average precipitate radius, and  $\theta \approx (2/3)(\Delta a/a)$  is the constrained lattice parameter mismatch, with  $\Delta a/a = 0.0125$  as the lattice parameter mismatch at room temperature [41]. Finally, strengthening by modulus mismatch is given as follows:

$$\sigma_{\text{mod}} = 0.0055M(\Delta G)^{3/2}\left(\frac{2\theta}{Gb^2}\right)^{1/2}b\left(\frac{r}{b}\right)^{\frac{3m}{2}-1} \quad (6)$$

where  $\Delta G = 42.5 \text{ GPa}$  is the shear modulus mismatch between the matrix and the precipitates [48], and  $m$  is a constant taken to be 0.85 [49].

The increase in yield strength due to Orowan dislocation looping is calculated as:

$$\sigma_{\text{Or}} = M\frac{0.4Gb}{\pi\sqrt{1-\nu}}\frac{\ln\left(\frac{2r}{b}\right)}{\lambda} \quad (7)$$

where  $\nu = 0.34$  is the matrix Poisson's ratio, and  $\lambda$  is the inter-precipitate distance, which is taken as the square lattice spacing on parallel planes [41]:

$$\lambda = \left[ \left(\frac{3\pi}{4\theta}\right)^{1/2} - 1.64 \right] r \quad (8)$$

From the TEM results, we estimated the average radius and volume fraction of  $\text{Al}_3(\text{Sc,Zr})$  particles to be 2.92 nm and 0.19%, respectively. Given the size of the nano-particles,  $\text{Al}_3(\text{Sc,Zr})$  particles induce order strengthening. And from the above calculations, the precipitate strengthening arising from  $\text{Al}_3(\text{Sc,Zr})$  contributes to a strength increment of 100 ~ 104 MPa.

Therefore, the calculated room temperature yield strength is in the range 214 ~ 234 MPa, which is consistent with the experimental results.

At room temperature, the dislocation movement is mainly based on the slip of the base plane, and is hindered by the interaction between the precipitates and dislocations, the distortion stress field of solute atoms, grain boundary, etc. It is difficult for dislocations to climb so precipitates effectively hinder the dislocation motion. However, at high temperatures,

with the increase of thermal vibration amplitude and a decrease of binding force between atoms, it is easy to climb the dislocation, and the blocking effect of various factors at room temperature on the dislocation is reduced, which makes the strength of the alloy decrease [51]. The solution strengthening remains operational at higher temperatures but becomes less effective and is limited by the low low eutectic temperature of the Al-Mg system. In the alloy studied in this paper, Sc and Zr formed solid solution during casting solidification and precipitated into nano-particles during the aging process. Besides, particles also precipitated during solidification, thereby refining grains and pinning grain boundaries [52]. The nano-particles located in the matrix have a good thermal resistance. In this alloy, it is the nano-particle strengthening mechanism which is the leading strengthening mechanism at higher temperatures. On the other hand, with the addition of Ca, a network of  $\text{Al}_4\text{Ca}$  plates was formed, which shows perfect high-temperature stability. At high temperatures, the network can restrain grain growth, stabilize grain boundary, enhance grain boundary strengthening effect and increase high-temperature stability. Under the combined action of the above strengthening mechanisms shown schematically in Fig. 10, Al-Mg-Sc alloy with Ca exhibited the equivalent or better

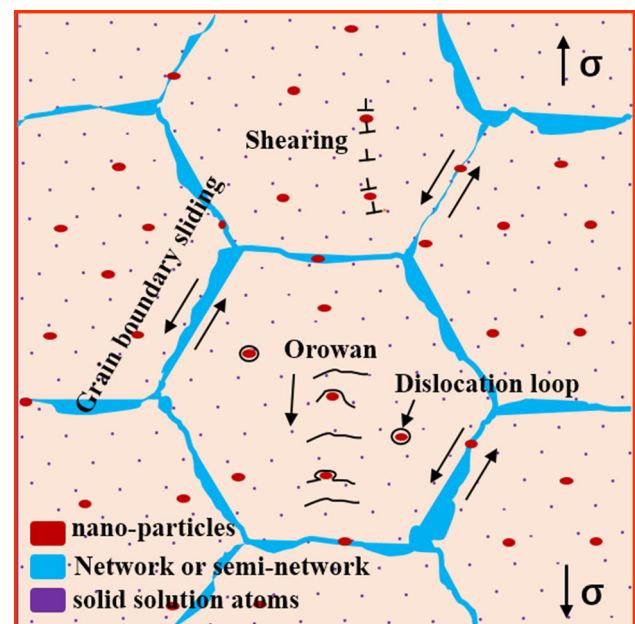


**Figure 10** Schematic representation of the hierarchical multiphase synergetic strengthening mechanism of Al-Mg-Sc modified with Ca under stress at elevated temperature.

mechanical properties of commercial alloys A356 and A319 at elevated temperatures. Moreover, it should be pointed out that for the solidification conditions used the strengthening mechanism could be made operational starting from the as-cast microstructure and a prior solution treatment was not necessary. The absence of a homogenization step reduces the power consumption during the alloy production process and reduces the number of production quality issues.

## Conclusion

In this study, the microstructure and mechanical properties were studied for the Al–Mg–Sc–Ca alloy containing 1% Ca. A hierarchical structure of an Al<sub>4</sub>Ca network / semi-network structure near the grain boundaries and Al<sub>3</sub>(Sc,Zr) nano-particles in the grain interior in combination with a high solute level was achieved. Following conclusions could be drawn from this study:

- (1) The Al<sub>4</sub>Ca network and Al<sub>3</sub>(Sc,Zr) nano-particles maintain high thermal stability and no obvious grain growth occurs when aging at temperatures 300~450 °C.
- (2) The ultimate tensile strength and yield strength of the heat-treated alloy reaches 259MPa, 216MPa at 150 °C, 175MPa and 160 MPa at 250 °C, and 136 MPa, 114 MPa at 300 °C. These values are equal or higher than those for corresponding commercial A356 and A319 alloys. And due to the low density of Ca, the alloy presented here shows a superior specific high-temperature strength.
- (3) The excellent high-temperature strength of the Ca-modified Al–Mg–Sc alloy is mainly derived from a hierarchical multi-factors strengthening, including the synergistic effect of grain boundary strengthening of Al<sub>4</sub>Ca network / semi-network, nanoparticle strengthening of Al<sub>3</sub>(-Sc,Zr), and solid solution strengthening of solute atoms.

## Acknowledgements

The authors are grateful for the financial supports by the National Natural Science foundation of China (Grant No. 51701095).

## Author contribution

HD was involved in conceptualization, formal analysis, investigation, data curation, writing–original draft and editing. SZ contributed to conceptualization, project administration, funding acquisition, writing–review and editing. BZ was involved in investigation, data curation. XT contributed to data curation. ZY was involved in resources, supervision. NB contributed to software, data curation, writing–reviewing. SZ was involved in writing–reviewing and Editing. ZL contributed to resources, validation.

## Declarations

**Conflicts of interest** The authors declare that they have no conflict of interest.

## References

- [1] Hirsch J (2011) Aluminium in innovative light-weight car design. *Mater Trans* 52(5):818–824. <https://doi.org/10.2320/matertrans.L-MZ201132>
- [2] Shaji MC, Ravikumar KK, Ravi M, Sukumaran K (2013) development of a high strength cast aluminium alloy for possible automotive applications. *Mater Sci Forum* 765:54–58
- [3] Hirsch J, Al-Samman T (2013) Superior light metals by texture engineering: optimized aluminum and magnesium alloys for automotive applications. *Acta Mater* 61(3):818–843. <https://doi.org/10.1016/j.actamat.2012.10.044>
- [4] Zhang G, Zhang J, Li B, Cai W (2013) Double-stage hardening behavior and fracture characteristics of a heavily alloyed Al–Si piston alloy during low-cycle fatigue loading. *Mater Sci Eng: A* 561:26–33. <https://doi.org/10.1016/j.msea.2012.10.073>
- [5] Feng J, Ye B, Zuo L, Qi R, Wang Q, Jiang H, Huang R, Ding W (2017) Effects of Ni content on low cycle fatigue and mechanical properties of Al-12Si-0.9Cu-0.8Mg-xNi at 350 °C. *Mater Sci Eng A* 706:27–37. <https://doi.org/10.1016/j.msea.2017.08.114>
- [6] Yao D, Xia Y, Feng Q, Jiang Q (2011) Effects of La addition on the elevated temperature properties of the casting Al–Cu alloy. *Mater Sci Eng A* 528(3):1463–1466. <https://doi.org/10.1016/j.msea.2010.10.046>
- [7] Abdulwahab M, Madugu IA, Yaro SA, Hassan SB, Popoola API (2011) Effects of multiple-step thermal ageing treatment on the hardness characteristics of A356.0-type Al–Si–Mg

- alloy. *Mater Des* 32(3):1159–1166. <https://doi.org/10.1016/j.matdes.2010.10.028>
- [8] Lumley RN, Morton AJ, Polmear IJ (2002) Enhanced creep performance in an Al–Cu–Mg–Ag alloy through underaging. *Acta Mater* 50(14):3597–3608. [https://doi.org/10.1016/S1359-6454\(02\)00164-7](https://doi.org/10.1016/S1359-6454(02)00164-7)
- [9] Zhao WG, Wang JG, Zhao HL, Yao DM, Jiang QC (2009) High creep resistance behavior of the cast Al–Cu alloy modified by nano-scale PrxOy. *Mater Sci Eng A* 515:10–13. <https://doi.org/10.1016/j.msea.2009.03.080>
- [10] Choi SH, Sung SY, Choi HJ, Sohn YH, Han BS, Lee KA (2011) High temperature tensile deformation behavior of new heat resistant aluminum alloy. *Mater Trans* 8(52):1661–1666. <https://doi.org/10.2320/matertrans.M2011025>
- [11] Alkahtani S, Elgallad E, Tash M, Samuel A, Samuel F (2016) Effect of rare earth metals on the microstructure of Al–Si based alloys. *Mater* 9(1):45. <https://doi.org/10.3390/ma9010045>
- [12] Li Y, Wu Y, Zhao Q, Liu X (2009) Effect of co-addition of RE, Fe and Mn on the microstructure and performance of A390 alloy. *Mater Sci Eng A* 527:146–149. <https://doi.org/10.1016/j.msea.2009.07.039>
- [13] Booth-Morrison C, Seidman DN, Dunand DC (2012) Effect of Er additions on ambient and high-temperature strength of precipitation-strengthened Al–Zr–Sc–Si alloys. *Acta Mater* 60(8):3643–3654. <https://doi.org/10.1016/j.actamat.2012.02.030>
- [14] Bao L, Wang H, Jie J, Wei Z (2011) Effects of yttrium and heat treatment on the microstructure and tensile properties of Al–7.5Si–0.5Mg alloy. *Mater Des* 32(3):1617–1622. <https://doi.org/10.1016/j.matdes.2010.08.040>
- [15] Hernandez-Sandoval J, Garza-Elizondo GH, Samuel AM, Valtierra S, Samuel FH (2014) The ambient and high temperature deformation behavior of Al–Si–Cu–Mg alloy with minor Ti, Zr, Ni additions. *Mater Des* 58:89–101. <https://doi.org/10.1016/j.matdes.2014.01.041>
- [16] Manasijevic S, Radisa R, Markovic S, Acimovic-Pavlovic Z, Raic K (2011) Thermal analysis and microscopic characterization of the piston alloy AlSi13Cu4Ni2Mg. *Intermetallics* 19:486–492. <https://doi.org/10.1016/j.intermet.2010.11.011>
- [17] Lathabai S, Lloyd PG (2002) The effect of scandium on the microstructure, mechanical properties and weldability of a cast Al–Mg alloy. *Acta Mater* 50(17):4275–4292. [https://doi.org/10.1016/S1359-6454\(02\)00259-8](https://doi.org/10.1016/S1359-6454(02)00259-8)
- [18] Kendig KL, Miracle DB (2002) Strengthening mechanisms of an Al–Mg–Sc–Zr alloy. *Acta Mater* 50(16):4165–4175. [https://doi.org/10.1016/S1359-6454\(02\)00258-6](https://doi.org/10.1016/S1359-6454(02)00258-6)
- [19] Vo NQ, Dunand DC, Seidman DN (2014) Improving aging and creep resistance in a dilute Al–Sc alloy by microalloying with Si, Zr and Er. *Acta Mater* 63:73–85. <https://doi.org/10.1016/j.actamat.2013.10.008>
- [20] Deng Y, Yin Z, Pan Q, Xu G, Duan Y, Wang Y (2017) Nanostructure evolution of secondary Al<sub>3</sub>(Sc<sub>1-x</sub>Zr<sub>x</sub>) particles during superplastic deformation and their effects on deformation mechanism in Al–Zn–Mg alloys. *J Alloys Compd* 695:142–153. <https://doi.org/10.1016/j.jallcom.2016.10.094>
- [21] Xu G, Qian J, Xiao D, Deng Y, Lu L, Yin Z (2016) Mechanical properties and microstructure of TIG and FSW joints of a new Al–Mg–Mn–Sc–Zr alloy. *J Mater Eng Perform* 25(4):1249–1256. <https://doi.org/10.1007/s11665-016-1942-6>
- [22] Røyset J, Ryum N (2013) Scandium in aluminium alloys. *Int Mater Rev* 50(1):19–44. <https://doi.org/10.1179/174328005X14311>
- [23] Zhang WG, Ye YC, He LJ, Li PJ, Feng X, Novikov LS (2013) Dynamic response and microstructure control of Al–Sc binary alloy under high-speed impact. *Mater Sci Eng A* 578:35–45. <https://doi.org/10.1016/j.msea.2013.04.067>
- [24] Kaiser MS, Datta S, Roychowdhury A, Banerjee MK (2008) Effect of scandium additions on the tensile properties of cast Al–6Mg alloys. *J Mater Eng Perform* 17(6):902–907. <https://doi.org/10.1007/s11665-008-9242-4>
- [25] Asghar Z, Requena G, Boller E (2011) Three-dimensional rigid multiphase networks providing high-temperature strength to cast AlSi10Cu5Ni1-2 piston alloys. *Acta Mater* 59(16):6420–6432. <https://doi.org/10.1016/j.actamat.2011.07.006>
- [26] Zhou DW, Liu JS, Peng P, Chen L, Hu YJ (2008) A first-principles study on the structural stability of Al<sub>2</sub>Ca Al<sub>4</sub>Ca and Mg<sub>2</sub>Ca phases. *Mater Lett* 62(2):206–210. <https://doi.org/10.1016/j.matlet.2007.04.110>
- [27] Mondal DP, Jha N, Badkul A, Das S, Yadav MS, Jain P (2011) Effect of calcium addition on the microstructure and compressive deformation behaviour of 7178 aluminium alloy. *Mater Des* 32(5):2803–2812. <https://doi.org/10.1016/j.matdes.2010.12.056>
- [28] Chen Y, Jin L, Fang D, Song Y, Ye R (2015) Effects of calcium, samarium addition on microstructure and mechanical properties of AZ61 magnesium alloy. *J Rare Earth* 33(1):86–92. [https://doi.org/10.1016/S1002-0721\(14\)60387-2](https://doi.org/10.1016/S1002-0721(14)60387-2)
- [29] Kumari S, Pillai RM, Nogita K, Dahle AK, Pai BCT (2006) Influence of calcium on the microstructure and properties of an Al–7Si–0.3Mg–xFe alloy. *Metall Mater Trans A* 37A:2581–2587. <https://doi.org/10.1007/BF02586230>
- [30] Huang L, Wang H, Yang DH, Ye F, Wang SQ, Lu ZP (2014) Effects of calcium on mechanical properties of cellular Al–Cu foams. *Mater Sci Eng A* 618:471–478. <https://doi.org/10.1016/j.msea.2014.09.051>

- [31] Akopyan TK, Letyagin NV, Sviridova TA, Korotkova NO, Prosviryakov AS (2020) New casting alloys based on the Al+Al<sub>4</sub>(Ca, La) Eutectic. *JOM-US* 72:3779–3786. <https://doi.org/10.1007/s11837-020-04340-z>
- [32] Belov NA, Naumova EA, Alabin AN, Matveeva IA (2015) Effect of scandium on structure and hardening of Al–Ca eutectic alloys. *J Alloys Compd* 646:741–747. <https://doi.org/10.1016/j.jallcom.2015.05.155>
- [33] Belov N, Naumova E, Akopyan T (2016) Eutectic alloys based on the Al–Zn–Mg–Ca system: microstructure, phase composition and hardening. *Mater Sci Technol* 33(6):656–666. <https://doi.org/10.1080/02670836.2016.1229847>
- [34] Naumova EA (2018) Use of calcium in alloys: from modifying to alloying. *Russ J Non-Ferr Met+* 59(3):284–298. <https://doi.org/10.17073/0021-3438-2018-2-59-76>
- [35] Norman AF, Prangnell PB, McEwen RS (1998) The solidification behaviour of dilute aluminium–scandium alloys. *Acta Mater* 46(16):5715–5732. [https://doi.org/10.1016/S1359-6454\(98\)00257-2](https://doi.org/10.1016/S1359-6454(98)00257-2)
- [36] Pan D, Zhou S, Zhang Z, Li M, Wu Y (2017) Effects of Sc(Zr) on the microstructure and mechanical properties of as-cast Al–Mg alloys. *Mater Sci Technol* 33(6):751–757. <https://doi.org/10.1080/02670836.2016.1270573>
- [37] Spierings AB, Dawson K, Heeling T, Uggowitzer PJ, Schäublin R, Palm F, Wegener K (2017) Microstructural features of Sc- and Zr-modified Al–Mg alloys processed by selective laser melting. *Mater Des* 115:52–63. <https://doi.org/10.1016/j.matdes.2016.11.040>
- [38] Akopyan TK, Belov NA, Naumova EA, Letyagin NV, Sviridova TA (2020) Al-matrix composite based on Al–Ca–Ni–La system additionally reinforced by L<sub>12</sub> type nanoparticles. *T Nonferr Metal Soc* 30(4):850–862. [https://doi.org/10.1016/S1003-6326\(20\)65259-1](https://doi.org/10.1016/S1003-6326(20)65259-1)
- [39] Luo X, Fang H, Liu H, Yan Y, Zhu H, Yu K (2019) Effect of Sc and Zr on Al<sub>6</sub>(Mn, Fe) phase in Al–Mg–Mn alloys. *Mater Trans* 60(5):737–742. <https://doi.org/10.2320/matertrans.M2018392>
- [40] Liang SS, Wen SP, Xu J, Wu XL, Gao KY, Huang H, Nie ZR (2020) The influence of Sc–Si clusters on aging hardening behavior of dilute Al–Sc–(Zr)–(Si) alloy. *J Alloys Compd* 842:1–6. <https://doi.org/10.1016/j.jallcom.2020.155826>
- [41] Seidman DN, Marquis EA, Dunand DC (2002) Precipitation strengthening at ambient and elevated temperatures of heat-treatable Al(Sc) alloys. *Acta Mater* 50(16):4021–4035. [https://doi.org/10.1016/S1359-6454\(02\)00201-X](https://doi.org/10.1016/S1359-6454(02)00201-X)
- [42] Aziz AM, Omar MZ, Sajuri Z (2020) Strength of thixoformed A319 alloy at elevated temperature. *Met Mater Int*. <https://doi.org/10.1007/s12540-019-00596-6>
- [43] Emadi D, Rao AKP, Mahfoud M (2010) Influence of scandium on the microstructure and mechanical properties of A319 alloy. *Mater Sci Eng A* 527(23):6123–6132. <https://doi.org/10.1016/j.msea.2010.06.042>
- [44] Azadi M, Shirazabad MM (2013) Heat treatment effect on thermo-mechanical fatigue and low cycle fatigue behaviors of A356.0 aluminum alloy. *Mater Des* 45:279–285. <https://doi.org/10.1016/j.matdes.2012.08.066>
- [45] Rincón E, López HF, Cisneros MM, Mancha H, Cisneros MA (2007) Effect of temperature on the tensile properties of an as-cast aluminum alloy A319. *Mater Sci Eng A* 452–453:682–687. <https://doi.org/10.1016/j.msea.2006.11.029>
- [46] Kim KJ, Jeong CY (2016) Effect of microstructure on high temperature mechanical properties of A319 casting alloy for automotive cylinder heads. *Mater Trans* 57(5):738–747. <https://doi.org/10.2320/matertrans.M2015402>
- [47] Cseh G, Bär J, Gudladt HJ, Lendvai J, Juhász A (1999) Indentation creep in a short fibre-reinforced metal matrix composite. *Mater Sci Eng A* 272(1):145–151. [https://doi.org/10.1016/S0921-5093\(99\)00466-9](https://doi.org/10.1016/S0921-5093(99)00466-9)
- [48] Vo NQ, Dunand DC, Seidman DN (2012) Atom probe tomographic study of a friction-stir-processed Al–Mg–Sc alloy. *Acta Mater* 60(20):7078–7089. <https://doi.org/10.1016/j.actamat.2012.09.015>
- [49] Krug ME, Mao Z, Seidman DN, Dunand DC (2014) Comparison between dislocation dynamics model predictions and experiments in precipitation-strengthened Al–Li–Sc alloys. *Acta Mater* 79:382–395. <https://doi.org/10.1016/j.actamat.2014.06.038>
- [50] Li R, Wang M, Li Z, Cao P, Yuan T, Zhu H (2020) Developing a high-strength Al–Mg–Si–Sc–Zr alloy for selective laser melting: crack-inhibiting and multiple strengthening mechanisms. *Acta Mater* 193:83–98. <https://doi.org/10.1016/j.actamat.2020.03.060>
- [51] Marquis EA, Seidman DN, Dunand DC (2003) Effect of Mg addition on the creep and yield behavior of an Al–Sc alloy. *Acta Mater* 51(16):4751–4760. [https://doi.org/10.1016/S1359-6454\(03\)00288-X](https://doi.org/10.1016/S1359-6454(03)00288-X)
- [52] Røyset J, Ryum N (2005) Kinetics and mechanisms of precipitation in an Al–0.2wt.% Sc alloy. *Mater Sci Eng A* 396:409–422. <https://doi.org/10.1016/j.msea.2005.02.015>

**Publisher's Note** Springer Nature remains neutral with regard to jurisdictional claims in published maps and institutional affiliations.